RESEARCH ARTICLE

Coagulation-flocculation of turbid water using graphene oxide: simulation through response surface methodology and process characterization

Nazila Rezania[1] · Maryam Hasani Zonoozi[1] · Motahareh Saadatpour[1]

Abstract

It was aimed to precisely investigate the coagulation properties of graphene oxide (GO) as a novel coagulant for turbidity removal from water. For this purpose, the process was simulated through response surface methodology (RSM) to determine the effect of the preselected independent factors (pH, GO dosage, and initial turbidity) and their interaction effects on the process. Based on the results, increased turbidity removal efficiencies were obtained as pH decreased from 10 to 3. Besides, increase of GO dosage within the test range (2.5–30 mg/L) was highly beneficial for enhancing the process performance. However, a slight overdosing of GO was observed for dosages of more than 20 mg/L under pH values of less than about 4. For initial turbidity with test range of 25–300 NTU, there was an optimum range (approximately 120–200 NTU) out of which the removal efficiency declined. According to the results of the analysis of variance (ANOVA), pH and GO dosage, orderly, had the strongest individual effect on the process performance. The most significant interaction effect was also observed between pH and GO dosage. The optimal coagulation conditions with GO dosage of 4.0 mg/L, pH of 3.0, and initial turbidity of 193.34 NTU led to a turbidity removal efficiency of about 98.3%, which was in good agreement with RSM results. Under basic pH levels, the sweeping effect was recognized as the main coagulation mechanism occurred between the negatively surface charged particles of GO and soil. However, according to zeta potential (ZP) analysis results, under acidic pH conditions in addition to the sweep coagulation, the electric double layer compression, and the subsequent ZP reduction also contributed significantly to the process. Scanning electron microscopy (SEM) images showed that the layered structure of GO particles provided an appropriate platform on which the flocs were formed.

Keywords Graphene oxide (GO) · Coagulation-flocculation process · Turbidity removal · Response surface methodology (RSM) · Sweep coagulation · Zeta potential reduction

Introduction

Surface water resources usually contain several organic and inorganic colloidal particles such as clay, silt, and

✉ Maryam Hasani Zonoozi
  mhzonoozi@iust.ac.ir; maryamzonooz@yahoo.com

  Nazila Rezania
  nazila_rezania@civileng.iust.ac.ir; nazilarezania@gmail.com

  Motahareh Saadatpour
  msaadatpour@iust.ac.ir

[1] Department of Civil Engineering, Iran University of Science and Technology (IUST), Narmak, Tehran 16846-13114, Iran

microorganisms. These suspended impurities reduce water transparency and make the water turbid (Reynolds and Richards 1996; Qasim et al. 2002; Altaher 2012; Aboubaraka et al. 2017). Colloidal particles typically have a net negative surface charge. Their large specific surface area (total surface area of a material per unit of mass) provides them with intensified surface effects. This results in strong repelling forces of the electrical charge between the particles and keeps the particles in a stable suspended condition (Metcalf and Eddy 2003). In the most water treatment plants, the two-step coagulation (chemical phase) and flocculation (physical phase) process is used to destabilize and remove colloidal particles (Jiang 2015). In coagulation phase, the repulsive force between the colloidal particles is reduced by chemical coagulants through different mechanisms depend

upon the coagulant type. Overcoming the repulsive force causes the colloidal particles to aggregate and form small flocs. After that, during the flocculation phase, collision of small flocs to each other results information of larger and more massive flocs which can be removed through gravity sedimentation (Metcalf and Eddy 2003; Baghvand et al. 2010). Traditionally, metal-based mineral coagulants such as aluminum and iron salts and synthetic polymers such as polyaluminium chloride (PACl) and polyacrylamide derivatives have been widely investigated for their application in water treatment works. Van Benschoten and Edzwald (1990) studied the chemical aspects and hydrolytic reactions of aluminum salts. Kang et al. (2003) evaluated the antimony removal from surface water using PACl and ferric chloride. Rizzo et al. (2005) evaluated the effectiveness of aluminium sulphate (alum), ferric chloride, and PACl for removal of natural organic matter (NOM) as precursors of trihalomethanes from surface water. Rizzo et al. (2008) compared the efficiency of chitosan and conventional coagulants (alum and ferric chloride) in turbidity and NOM removal from surface water. Yang et al. (2010) studied the pH effect on coagulation performance of Al-based coagulants and residual aluminum for the removal of humic acid and kaolin from water. Jiang and Wang (2009) compared the performance of polyferric chloride and ferric chloride for the removal of humic acid from water. Guo et al. (2015) investigated the coagulation performance and floc characteristics of alum with cationic polyamidine as coagulant-aid for removal of kaolin and humic acid from synthetic test water.

Although the cost-effectiveness of these traditional coagulants and their acceptable performance in removal of turbidity, NOM, and some other pollutants from water has turned them into the most extensively applied coagulants in water treatment processes, due to some of their health and environmental effects, utilization of new alternatives with less side effects, and high effectiveness has always been a concern (Divakaran and Pillai 2002; Zhu et al. 2011; Yang et al. 2013; Huang et al. 2016; Aboubaraka et al. 2017).

Graphene oxide (GO) is a two-dimensional carbon–based nanomaterial that has been recently studied for water and wastewater treatment purposes, thanks to its remarkable surface properties (Tan et al. 2017; Hiew et al. 2019; Jin et al. 2019). Because of its two-dimensional structure, GO has shown a high capability for absorption of soluble contaminants from water (Zhao et al. 2011a; Zhao et al. 2011b). GO possesses various oxygen-containing groups on its surface including hydroxyl, carboxyl, carbonyl, and epoxy. These functional groups improve the aqueous dispersibility of the GO and emphasize its surface properties (Park and Ruoff 2009; Yang et al. 2012a; Hiew et al. 2019). At the moment, the average price per unit mass of GO can be more than 500,000 times the average price per

unit mass of Alum, depend upon the producer and the product specifications. However, with the development of technology, it has the great potential for large-scale and cost-effective production (Yang et al. 2013; Aboubaraka et al. 2017). It is also worth mentioning that the biodegradability of the GO in the presence of some enzymes has been proven according to some previous researches (Sanchez et al. 2011).

Considerable studies (Ramesha et al. 2011; Yang et al. 2011; Zhao et al. 2011b; Li et al. 2012; Robati et al. 2016) have been carried out on the elimination of soluble pollutants using GO as an adsorbent. However, very few studies (Yang et al. 2013; Aboubaraka et al. 2017) have been performed recently on GO performance as a coagulant. Yang et al. (2013) and Aboubaraka et al. (2017) investigated the coagulation ability of GO for removal of different contaminants from water. Although, both studies have been performed based on OFAT method (one factor at a time), and experimental design methods have not been used. For this reason, the interaction effects of the operational parameters on GO coagulation properties as well as some other aspects of the subject are neglected.

On the other hand, the appropriate implementation of coagulation-flocculation process severely depends on precise choosing of the effective factors and their values. Response surface methodology (RSM) is one of the most appropriate multivariant techniques used for multivariant experimental design, analysis, statistical modeling, and process optimization. This methodology allows evaluating and deducing the individual and the interaction effects of several factors on the desired response. Using RSM, a lot of information can be achieved about a process through a minimum number of experiments (Kirmizakis et al. 2014; Nourani et al. 2016; Ooi et al. 2018; Adesina et al. 2019; Zhao et al. 2019; Krishnan et al. 2020).

The main aim of the present work is to precisely investigate the coagulation properties of GO for turbidity removal from water. It was focused on the process simulation using RSM to determine the effect of the individual factors as well as the influences of their interaction on the process. For this purpose, experiments were conducted using jar test instrument. The effect of different factors including pH, coagulant dosage, initial turbidity, and rapid and slow mixing time was examined. The relationship between turbidity removal efficiency and three independent parameters including pH, initial turbidity, and GO dosage were evaluated by applying central composite design (CCD) in RSM. Besides, optimization of the process conditions was carried out by applying RSM analysis. In order to more precisely characterize the process, scanning electron microscopy (SEM), energy dispersive X-ray spectroscopy (EDX), particle size distribution (PSD), zeta potential (ZP), and other analyzes were performed.

Materials and methods

Materials

Single-layer GO, with a layer thickness of 0.7–1.4 nm, was purchased in form of a suspension from GrapheneX company (Iran). It had been synthesized using Modified Hummers Method (Hummers Jr and Offeman 1958). UV-Vis absorption spectra of the GO showed an intense peak at about 228 nm (λ_{max}). Turbid samples were prepared using tap water and garden soil passed the sieve No. 200 (particles smaller than 0.075 mm). Characteristics of the used tap water are shown in Table 1. Hydrochloric acid (HCl) and sodium hydroxide (NaOH) from Merck Company (Germany) were used for pH adjustment.

Coagulation-flocculation procedure

The soil particles passed through sieve No. 200 were dispersed in 2 L of tap water. To separate fine aggregates adhered to each other and obtain a uniform dispersion, the stock suspension was stirred at 100 rpm for 1 h. The suspension was then left for 24 h for complete hydration of the particles. After that, the stock suspension was stirred again and allowed to settle for 60 min. The obtained supernatant was used to prepare different levels of turbidity. Turbidity was measured using Milwaukee Turbidity meter (Mi415, Romania). The pH of the samples was adjusted using 0.1 M HCl and 0.1 M NaOH solutions. A CyberScan PC 300 Portable pH-meter (Eutech Instruments, Singapore) was used for pH measurement. A six-paddle jar test apparatus (HACH, Germany) was used for coagulation and flocculation tests. All experiments were performed in 600-mL beakers at room temperature. The beakers were filled with 400 mL of the prepared turbid water samples. To implement the coagulation and flocculation phases, the samples were first agitated at rapid mixing rate of 200 rpm for 2 min and then were slowly stirred at 50 rpm for 15 min. The turbidity removal efficiency was calculated using the following equation:

$$\text{Turbidity removal } (\%) = \frac{T_0 - T}{T_0} \times 100 \quad (1)$$

where, T_0 and T are the turbidity values of the sample before and after the process, respectively.

Table 1 Characteristics of the used tap water

Turbidity (NTU)	pH	EC[1] (μS/cm)	TDS[2] (ppm)
0.8 ± 0.13	7.6 ± 0.12	279 ± 17.6	137 ± 12.2

[1] Electrical conductivity, [2] Total dissolved solids

Pretests

As the first step, preliminary experiments were conducted to determine the most effective parameters on the coagulation properties of GO for turbidity removal from water and as well, to identify the effective ranges of those parameters for the experimental design step. For this purpose, the effect of pH, GO dosage, initial turbidity, rapid mixing time, and slow mixing time on the removal efficiency was evaluated.

The results showed that decreasing pH from 11 to 3, and as well, increasing GO dosage from 2.5 to 30 mg/L enhanced the turbidity removal efficiency. However, changing the initial turbidity within the range of 25–300 NTU did not show a vivid independent effect which seemed to be influenced by the GO dosage and specially the pH value. On the contrary, in many previous studies on pollutant removal using coagulation process, the initial concentration of the contaminant has been distinguished as an important independent variable (Anouzla et al. 2009; Sadri Moghaddam et al. 2011; Aslani et al. 2016; Zhao et al. 2019). Therefore, despite the obtained result of the OFAT tests, it seemed necessary to more accurately investigate the individual effects of the initial turbidity and its interactions with the two other parameters, through experimental design method. For this reason, this parameter was considered as one of the RSM input parameters. Changing the rapid and slow mixing times within the ranges of 1–5 min and 10–40 min, respectively, had a negligible effect on removal efficiency. This was most probably due to the high specific surface area of GO which provides sufficient contact between the GO and the colloidal particles and consequently, minimizes the need for mechanical mixing. Accordingly, coagulant dosage (GO dosage), initial pH, and initial turbidity were chosen as the most effective independent variables in the coagulation-flocculation process.

Experimental design and data analysis

As described by Trinh and Kang (2011), the relationship between the responses and the independent variables in coagulation-flocculation process cannot be well modeled by zero- and first-order models, while second-order models properly approximate the desired responses. For this reason, a central composite design (CCD), which is an efficient design tool for fitting the second-order models (Montgomery 2001), was used for RSM in experimental design. To design the experimental runs and analyze the obtained data, Design Expert software (version 7.0.0) was employed. The predetermined effective ranges of the chosen independent variables, i.e., coagulant dosage, initial pH of the samples, and initial turbidity, are presented in Table 2 in both coded and actual mode. A CCD containing 20 experiments, with 8 star points (coded to the usual ± 1 notation), 6 axial points corresponding to the alpha value (($\pm \alpha$, 0, 0), (0, $\pm \alpha$, 0), (0, 0, $\pm \alpha$)), and 6

Table 2 The levels of independent variables in terms of actual unit of measurement and coded unit

Variables	Symbol	Levels				
		$-\alpha$	-1	0	1	$+\alpha$
Initial turbidity (NTU)	X_1	25	80.74	162.5	244.26	300
pH	X_2	3	4.42	6.5	8.58	10
GO dosage (mg/L)	X_3	2.5	8.07	16.25	24.43	30

replicates at the center points (0, 0, 0) were used to build quadratic models. The value of α depends on the number of variables and is calculated according to Eq. 2.

$$\alpha = \left(2^k\right)^{1/4} \tag{2}$$

where, k is the number of variables. Using Eq. 2, α is equal to 1.682.

For modeling and explaining the process behavior, a second-order polynomial function (as shown in Eq. 3) was fitted to the obtained experimental data.Equation ID=b=t

$$Y = \beta_0 + \sum_{i=1}^{n}\beta_i x_i + \sum_{i=1}^{n}\beta_{ii} x_i^2 + \sum_{i=1}^{n}\sum_{j=1}^{n}\beta_{ij} x_i x_j \tag{3}$$

where Y is the predicted response (turbidity removal efficiency); n the number of variables; x_i and x_j the coded values of the variables which influence predicted response; β_0 is the constant coefficient; β_i, β_{ii}, and β_{ij} are the coefficients of linear, quadratic, and interaction terms, respectively.

The adequacy of the proposed model was examined through diagnostic checking tests provided by analysis of variance (ANOVA) with 95% confidence interval. In this regard, the goodness of the polynomial model's fit was expressed by the coefficient of determination (R^2, correlation coefficient) and the model terms were evaluated using F value (Fisher's test) and P value (probability value).

Process optimization using desirability function

As well explained by Myers et al. (2009), the desirability function approach transforms an estimated response into a scale-free value, called desirability. This is a method for optimizing the processes with one or more responses. The general approach is to first convert each response y_i into a distinct desirability function d_i that varies over the range:

$$0 \leq d_i \leq 1. \tag{4}$$

where, if the response y_i is at its goal or target, then $d_i = 1$, and if the response is outside an acceptable region, $d_i = 0$. Then the design variables are chosen to maximize the overall desirability. The overall desirability function D (Eq. 5) is

defined as the geometric average of the individual desirability functions of each response, where m is the number of responses (Myers et al. 2009).

$$D = \left(d_1 d_2 \ldots d_m\right)^{1/m} \tag{5}$$

If the objective or target T for the response y is a maximum value, the individual desirability function is as follows (Myers et al. 2009):

$$d_i = \begin{cases} 0 & y_i < L_i \\ \left(\dfrac{y_i - L_i}{T_i - L_i}\right)^r & L_i \leq y_i \leq T_i \\ 1 & y_i > T_i \end{cases} \tag{6}$$

And if the target for the response is a minimum value, then (Myers et al. 2009):

$$d_i = \begin{cases} 1 & y_i < T_i \\ \left(\dfrac{U_i - y_i}{U_i - T_i}\right)^r & T_i \leq y_i \leq U_i \\ 0 & y_i > U_i \end{cases} \tag{7}$$

where, L and U are the lower and upper limits. Choosing $r > 1$ places more emphasis on being close to the target value, and choosing $0 < r < 1$ makes this less important. The two-sided desirability assumes that the target is located between the lower (L) and upper (U) limits, and is defined as (Myers et al. 2009):

$$d_i = \begin{cases} 0 & y_i < L_i \\ \left(\dfrac{y_i - L_i}{T_i - L_i}\right)^{r_1} & L_i \leq y_i \leq T_i \\ \left(\dfrac{U_i - y_i}{U_i - T_i}\right)^{r_2} & T_i \leq y_i \leq U_i \\ 0 & y_i > U_i \end{cases} \tag{8}$$

The Design Expert software uses direct search methods to maximize the desirability function D (Myers et al. 2009).

In this study, the process variables were optimized using the optimization function of the Design Expert software with desirability approach. As seen in Table 3, to optimize the process variables, the desired goal for both initial pH and initial turbidity was set as "in range", while GO dosage was set to be minimized due to the high price of the GO nanomaterial. Some researchers have similarly chosen the

Table 3 Aims and ranges of the optimization analysis

Parameter	Aim	Lower and upper limits
Initial pH	In range	3–10
Initial turbidity (NTU)	In range	25–300
GO dosage (mg/L)	Minimize	2.5–30
Turbidity removal efficiency (%)	Maximize	90–100

"least possible" constraint for costly parameters such as coagulant dosage (Daud et al. 2018). However, depending upon the nature of the process and its effective parameters, some others have set the aim for all effective parameters as "in range" (Adesina et al. 2019; Krishnan et al. 2020). Maximizing the turbidity removal efficiency as the desired response (y), using the mentioned constraints was the goal of optimization.

Characterization tests

Optical microscope (Bell, Italy) was used to observe and compare the form and appearance of the soil particles and the formed flocs before and after the process, respectively. A scanning electron microscope (SEM) (Tescan vega II, Czech Republic) equipped with energy dispersive X-ray spectroscopy (EDX) was employed for characterizing the GO, soil, and flocs samples in terms of their morphological information and main constituents. To prepare the floc sample for SEM analysis, after coagulation-flocculation process and formation of the flocs, the supernatant of sample was gently removed using a pipette. Then, the flocs were softly placed on a slide and allowed to dry at room temperature. In the case of GO nanoparticles, the dried sample of the GO suspension with initial concentration of 50 ppm was used. The dried samples were then covered with a thin layer of gold, and their surfaces were observed by SEM apparatus. Particle size distribution of the initial turbid samples and the produced flocs was analyzed by dynamic light scattering on HORIBA SZ-100 (Japan) and Malvern Mastersizer 2000 (Worcestershire, UK), respectively. HORIBA SZ-100 (Japan) was also used for measuring zeta potential (ZP) of the initial turbid samples and the flocs (settled flocs after the process).

Results and discussion

Developing regression model equation and statistical analysis

In order to evaluate the combined effect of the process parameters consisting of initial turbidity, pH, and GO dosage, experiments were performed according to the combinations of the parameters' levels proposed by RSM through statistical experimental design. The experimental design matrix and the observed values of turbidity removal efficiency are presented in Table 4. The adequacy and significance of the proposed model and its terms were tested by ANOVA as presented in Table 5. The P values less than 0.05 indicate that the model terms are significant (Mora et al. 2019). Accordingly, the nonsignificant terms with P value > 0.05 were excluded by backward elimination procedure, and only statistically significant terms were used in the model. The proposed response

function in the form of a second order polynomial model is presented in Eq. 9. The terms with positive sign affect the response Y synergistically, whereas the negative terms have antagonistic effects.?]?]

Equation ID=b=t

$$Y = 92.56 + 2.16\,X_1 - 10.50\,X_2 + 5.62\,X_3 - 1.19\,X_1 X_2$$
$$+ 4.52\,X_2 X_3 - 5.50\,X_1{}^2 - 4.23\,X_2{}^2 - 1.56\,X_3{}^2 \qquad (9)$$

where, Y is the predicted turbidity efficiency (data given in Table 4), X_1, X_2, and X_3 are the coded variables corresponded to initial turbidity, pH, and GO dosage, respectively.

According to data of ANOVA analysis results in Table 5, the model and its linear terms (X_1, X_2, and X_3), quadratic terms ($X_1{}^2$, $X_2{}^2$, and $X_3{}^2$), and interactive terms ($X_1 X_2$ and $X_2 X_3$), which had P value below 0.05, were significant. Among three independent factors, pH (X_2), and GO dosage (X_3) were the most effective ones, orderly, according to their P values (less than 0.0001) and their high F values (833.23 for pH and 238.64 for GO Dosage). This result is in accordance with those reported by Simate et al. (2012) and Yang et al. (2012b) according to whom, coagulant dosage and pH are two of the most effective external factors in coagulation-flocculation performance.

In addition, the most significant interaction effect on the response Y belonged to term $X_2 X_3$ (pH and GO dosage) since it showed the lowest P value (0.0001) and the highest F value (90.51) amongst all interaction terms. Merely, the interaction term $X_1 X_3$ (initial turbidity and GO dosage) with P value > 0.05 was found to be insignificant and removed from the model.

Data of the model validation are presented in Table 5 and Fig. 1. As seen in the table, the model had a low P value of < 0.0001 and a high F value of 194.77 which imply that the proposed second-order polynomial model was significant for the turbidity removal efficiency. According to the lack-of-fit p value of 0.4213 > 0.05, the model does not suffer from lack-of-fit. Goodness-of-fit for the model was further evaluated by coefficients of determination R^2. Based on the ANOVA results, the model presents a high R^2 value of 99.30% which indicates that the model's accuracy and overall performance are satisfactory. The adjusted coefficient of determination (R^2_{adj}) was also high (98.79%). This means that 98.79% of the observed response values can be explained by the proposed model. Besides, the proximity of the values of R^2 and R^2_{adj} implies that there is very little chance that nonsignificant terms have been included in the model (Montgomery 2001). The predicted R^2 (R^2_{pred}) which describes the prediction capability of the model for new responses, was obtained 97.19%. Therefore, the model has very high capability for predicting new responses.

Table 4 CCD matrix and the obtained results

RUN	Initial turbidity (NTU)	pH	GO Dosage (mg/L)	Turbidity removal (%)	
				Experimental	Predicted
1	162.50	3.00	16.25	97.59	98.26
2	162.50	6.50	16.25	92.12	92.56
3	162.50	6.50	16.25	93.90	92.56
4	244.26	4.42	24.43	96.07	95.98
5	162.50	6.50	16.25	93.53	92.56
6	80.74	4.42	24.43	90.47	89.76
7	162.50	6.50	16.25	93.10	92.56
8	244.26	4.42	8.07	94.20	94.26
9	80.74	8.58	24.43	81.34	80.17
10	244.26	8.58	8.07	62.24	61.84
11	162.50	6.50	16.25	90.36	92.56
12	162.50	6.50	16.25	92.63	92.56
13	162.50	6.50	30.00	97.09	97.61
14	80.74	8.58	8.07	60.44	59.42
15	300.00	6.50	16.25	81.02	80.63
16	162.50	10.00	16.25	62.04	62.94
17	162.50	6.50	2.50	77.66	78.71
18	80.74	4.42	8.07	88.39	87.10
19	25.00	6.50	16.25	71.41	73.37
20	244.26	8.58	24.43	81.47	81.65

The normal probability plot of the studentized residuals is presented in Fig. 1a. As illustrated in the figure, all residues lie on a straight line which indicates the constancy of the variance and normal distribution of data. Figure 1b shows the plot of residuals versus predicted values according to which, the residuals are distributed without any systematic structure and show a random pattern on both sides of 0 line. The both plots reveal reasonably well-behaved residuals for the model and confirm the model's reliability and adequacy for describing turbidity removal efficiency using GO.

Table 5 ANOVA for turbidity removal efficiency using GO (%)

Source	Sum of squares	df[1]	Mean square	F value	P value
Model	2816.81	8	352.10	194.77	< 0.0001
X_1-Turbidity	63.73	1	63.73	35.25	< 0.0001
X_2-pH	1506.31	1	1506.31	833.23	< 0.0001
X_3-GO dosage	431.41	1	431.41	238.64	< 0.0001
X_1X_2	11.23	1	11.23	6.21	0.0299
X_2X_3	163.62	1	163.62	90.51	< 0.0001
X_1^2	436.31	1	436.31	241.35	< 0.0001
X_2^2	257.81	1	257.81	142.61	< 0.0001
X_3^2	34.92	1	34.92	19.32	0.0011
Residual	19.89	11	1.81		
Lack of Fit	11.83	6	1.97	1.22	0.4213
Pure Error	8.05	5	1.61		
Std. Dev.[2]	1.34		R^2	0.9930	
C. V. %[3]	1.58		R^2_{adj}	0.9879	
Adeq. precision[4]	42.806		R^2_{pred}	0.9719	

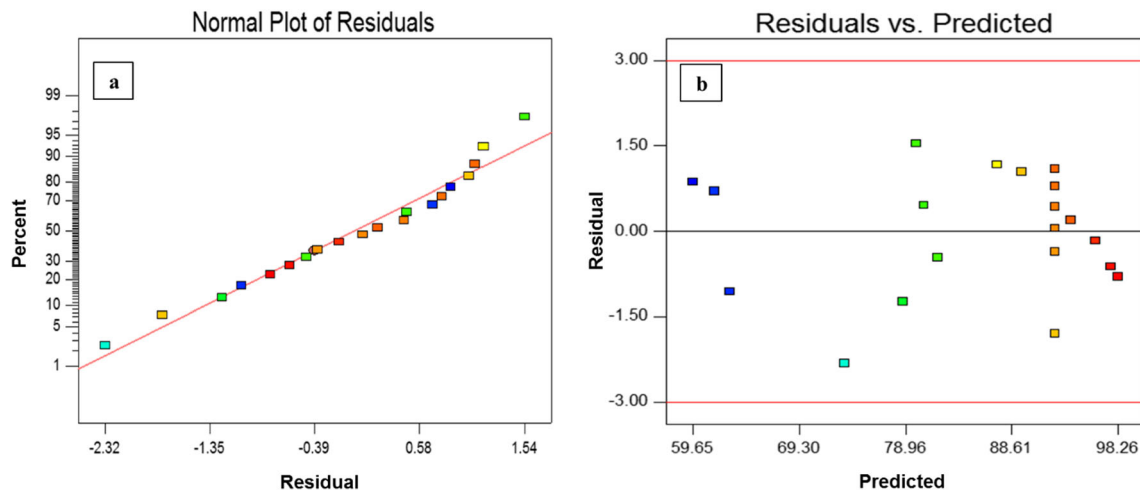[1] Degree of freedom, [2] Standard deviation, [3] Coefficient of variation, [4] Adequate precision

Fig. 1 Diagnostics plots: **a** Normal probability plot of residuals and **b** residuals versus predicted values

Response surface and contour plots

In order to provide a better explanation of the independent variables (operational parameters) and their interaction effects on turbidity removal, the response surface plots are represented in Fig. 2 in both 3D and contour formats.

Figure 2a represents the effects of initial turbidity (X_1) and pH (X_2) on the turbidity removal efficiency, while the coagulant dosage was kept at its central level (16.25 mg/L). Figure 2b depicts the effects of pH (X_2) and coagulant dosage (X_3) with the initial turbidity kept constant at 162.5 NTU.
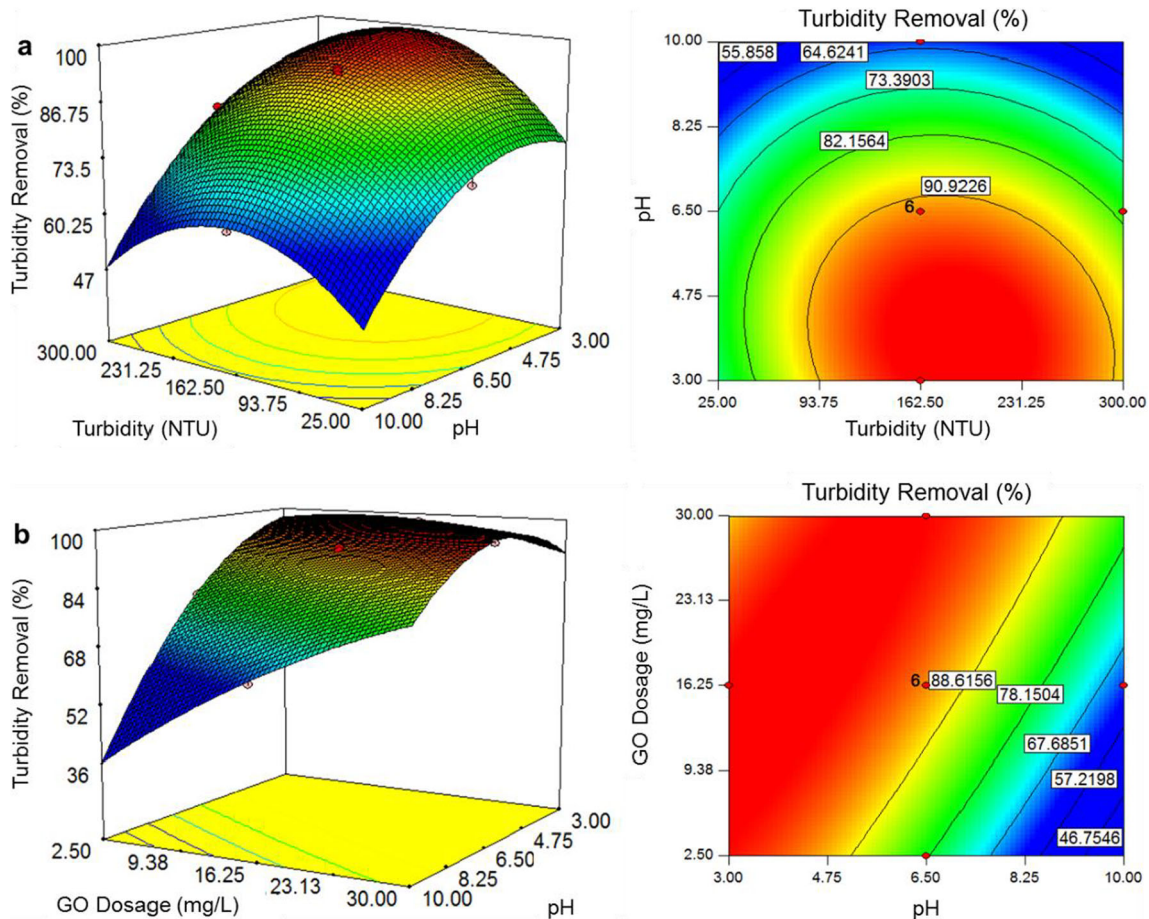

Fig. 2 Response surface and contour plots of **a** initial turbidity and pH, **b** pH and coagulant dosage

The individual effect of the parameters

Effect of pH As illustrated in Fig. 2a and 2b, pH decrease was generally beneficial for enhancing the turbidity removal efficiency. This result is consistent whit those reported by Yang et al. (2013) who studied on turbidity removal from Kaolin containing samples using GO at three pH levels of 4, 7, and 11 and observed the highest removal efficiency at the acidic pH of 4. Referring to the figures, in spite of the significant effect of pH on the process, high or very high turbidity removal efficiencies (70–100%) were achievable within a relatively wide pH range (3–8).

As the GO and most colloidal particles within the soil are both negatively surface charged (Bolt 1976; Jefferson et al. 2004; Liu et al. 2017; Tan et al. 2017), the sweep coagulation is thought to be the predominant floc formation mechanism within the process (Yang et al. 2013). However, according to the results of the present study, it is likely that the H^+ ions at acidic pH conditions have surrounded or reacted with both GO and soil particles and reduced the effect intensity of their negative charge. This may resulted in decrease of electrostatic repulsion force between GO and soil particles and made it possible for them to get closer together and have more collisions. In the other words, at low pH levels charge neutralization and electric double layer compression (decrease of ZP) may have occurred as coagulation mechanism. To better understand which of the mentioned mechanisms have occurred, final pH of some samples (pH at the end of the process) was measured. Figure 3 shows the final pH of the samples versus their initial pH values. As can be seen, a line with an approximate slope of 1.0 (0.945) fitted well ($R^2 = 0.9932$) to the points indicating that the final and the initial pH of the samples were approximately the same. This reveals that at acidic pH condition, the H^+ ions added to the medium have not bonded
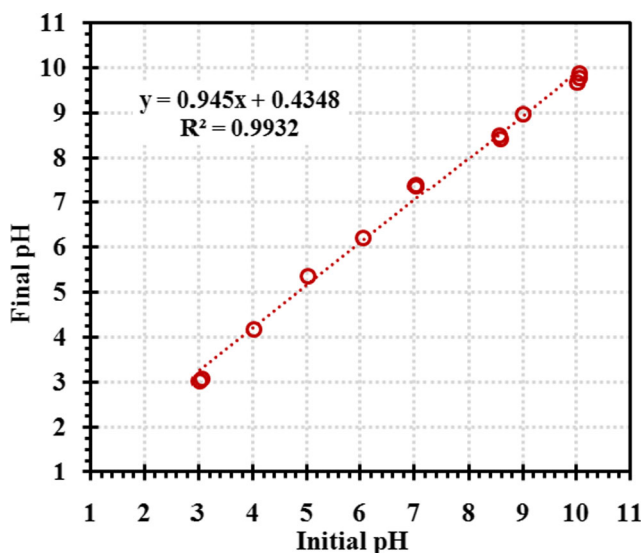

Fig. 3 Final pH of the samples versus initial pH values

or reacted with the GO or soil particles but solely surrounded them. This reveals that charge neutralization has barely contributed to the process; however, the electric double layer compression and the consequent ZP reduction have probably occurred. This subject is more discussed in the "Zeta potential analysis" section.

It is also worth mentioning that traditional coagulants such as aluminum sulfate (Alum), ferric chloride and polyaluminum chloride (PACl) have been reported to change the pH of the sample so that pH control and adjustment during and after the process is required (Qasim et al. 2002; Zhang et al. 2008; Baghvand et al. 2010; Yang et al. 2013). But according to the obtained results of the present study, using GO as coagulant, there is less need for pH control and adjustment throughout the process and after its completion. This can be considered as an advantage in GO performance over traditional coagulants.

Effect of GO dosage According to Fig. 2b with the increase of GO dosage within the test range, the removal efficiency increased steadily in most applied conditions so that the maximum turbidity removal efficiencies were mostly achieved at the maximum GO dosage of 30 mg/L. This can be attributed to the more collisions between the coagulant and the soil particles takes place at higher GO dosages. However, a slight overdosing of GO was observed for dosages of more than 20 mg/L under pH values of less than about 4 (Fig. 2b). This suggests that the effect of GO dosage depends on the pH level so that under improper pH conditions (approximately more than 6), increasing GO dosage helped the process and resulted in higher removal efficiencies while under optimum pH values (below 4) it affected adversely and decreased the process efficiency. Regarding the same surface charge of the GO and the soil particles, this decrease in the efficiency could not be referred to the re-stabilization of the soil particles. But it seems that under overdose conditions, the supernatant quality declined mostly due to excess part of the GO particles which did not participate in the process and remained suspended within the medium. The obtained result is not compatible with those reported by Yang et al. (2013) and Aboubaraka et al. (2017) according to whom, even high GO dosages of 25 mg/L and 48 mg/L, respectively, did not adversely affect the coagulation efficiency. The reason for this difference is probably because they conducted their studies solely on the basis of OFAT tests.

Effect of initial turbidity The effect of initial turbidity on the process performance is illustrated in Fig. 2a. According to the figure, there was an optimum range for turbidity out of which the removal efficiency slightly declined. The results suggest that at low turbidity levels, lack of collisions between the GO and the soil particles has led to the formation of fewer flocs. Therefore, part of the GO and the soil particle remained

suspended at the end of the process, thereby degrading the process performance. In contrast, at high turbidity levels, inadequacy of GO dosage relative to the pollutant concentration has reduced the process efficiency.

The interaction effect of the parameters

Interaction effect of pH and initial turbidity Figure 2a illustrates the interaction effect of pH and turbidity. According to the figure, under all turbidity levels, decreasing the pH increased the removal efficiency. This increase in efficiency was slightly higher at larger values of the initial turbidity. For example, at initial turbidity of 25 NTU, with pH decrease from 10 to 3, the removal efficiency increased from less than 55.86% to about 80.0%, while it rose from less than 55.86% to about 90.0% at initial turbidity of 300 NTU. The reason for this observation is probably that under higher turbidity levels, more soil particles were surrounded by H^+ ions. As a result, the process benefited more from the ZP reduction. Thus, higher removal efficiencies were obtained with pH decrease under higher turbidity values compared to the lower turbidity levels. The results represent a moderate interaction between pH and initial turbidity.

Interaction effect of pH and GO dosage The most severe interaction effect was attributed to the pH and the GO dosage. As seen in Fig. 2b, at initial pH of 3, with increase of GO dosage from 2.5 to 30 mg/L, the removal efficiency changed between about 90% to approximately 100%, while it increased from less than 46.75% to about 80.0% at initial pH of 10. In the other words, under optimum pH levels (highly acidic conditions), the removal efficiencies were very high, and the effect of GO dosage on the process performance was little, while, when pH was inappropriate (basic conditions), lower removal efficiencies were obtained, and GO dosage affected the process strongly. The reason for such a severe interaction effect can be attributed to the very high specific surface area of the GO particles. In fact, this characteristic caused a huge number of H^+ ions to accumulate around the GO particles under acidic pH values. This feature resulted in significant increase of the removal efficiency at very low GO dosages, while leaded to a negligible overdosing under higher GO dosages. Therefore, it can be said that under acidic pH conditions,

due to the abundance of H^+ ions around the GO sheets, ZP reduction alongside sweeping effect plays important role in coagulation, allowing high removal efficiencies to be obtained even with very low GO dosages. In contrast, at basic pH levels, lack of H^+ ions can be well compensated by higher GO dosages so that the same efficiencies can be gained through strong sweep coagulation.

Process optimization

The results of the process optimization are presented in Table 6. The very low concentration suggested for GO (4 mg/L) by the model is desirable and noteworthy. The model estimated 98.53% removal efficiency under the suggested optimal conditions at which a high desirability of 0.898 was reported. It should also be mentioned that if GO dosage was chosen in the range, higher values of removal efficiency and desirability would be obtained.?]

The predicted optimal conditions were tested in three replicates to validate the optimization results. The obtained value of $98.27 \pm 0.51\%$ was reasonably close to the predicted value of the model equation (98.53%) confirming the validity and accuracy of the optimization analysis results.

The 3D graph of desirability at optimal conditions is shown in Fig. 4. According to the figure, at the optimal GO dosage of 4 mg/L and pH values of more than 5, the desirability for all initial turbidity levels is zero. However, by decreasing pH from 5 to 3 and approaching the initial turbidity of 193 NTU, the desirability increases up to about 0.9. Turbidity levels of lower or higher than 193 NTU declines the desirability.

Figure 5 shows the removal of turbidity at GO dosage of 4 mg/L and confirms the desirability results. As can be seen, at all initial turbidity levels, pH reduction caused an increase in the removal efficiency. In addition, at all pH levels, the highest turbidity removal efficiencies were obtained for turbidity values of around 193 NTU.

### Characterization of soil, GO, and floc particles

Microscopic observations

Figure 6 represents the optical microscope images of a sample with initial turbidity and pH values of 162.5 NTU and 6.5, respectively, before and after coagulation-flocculation process
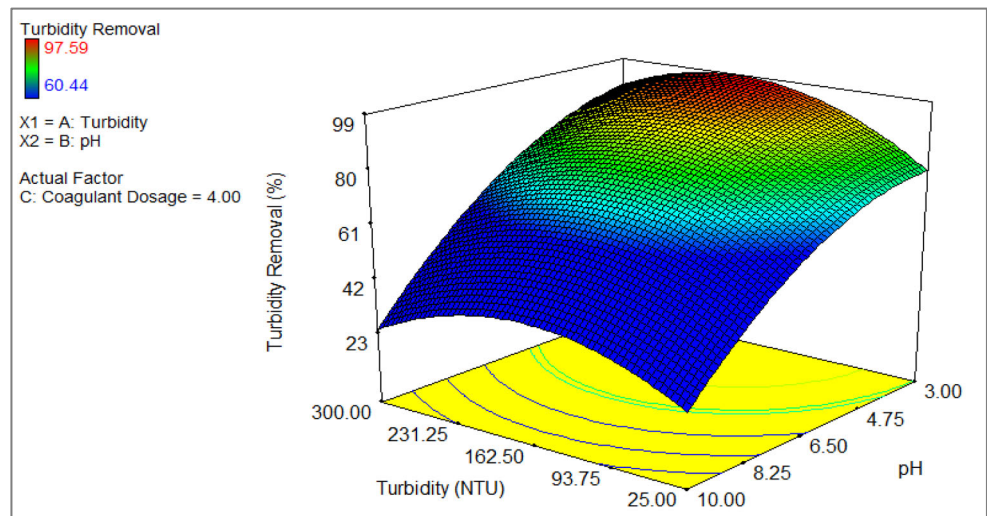
Table 6 Results of process optimization

|	Optimal conditions		Turbidity removal at optimal conditions		Desirability
pH	Initial turbidity (NTU)	GO dosage (mg/L)	Predicted (%)	Experimental (%)	
3	193.34	4	98.53	98.27 ± 0.51	0.898

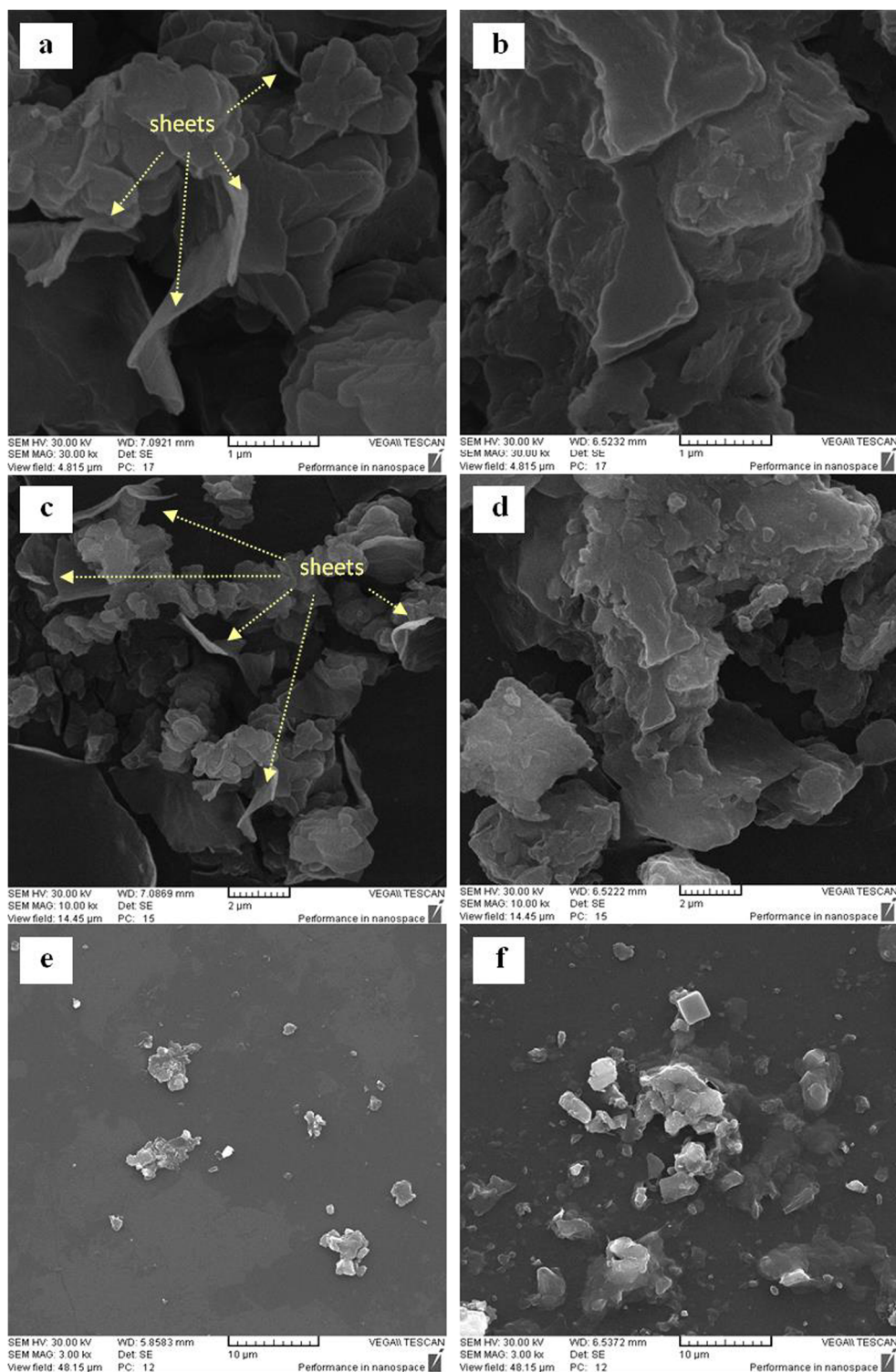**Fig. 4** Desirability at GO dosage of 4 mg/L
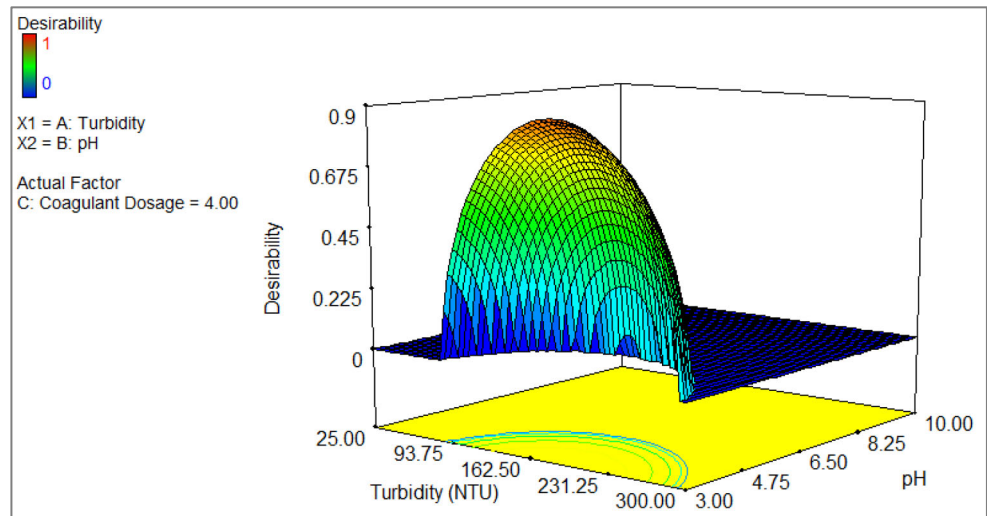
Fig. 5 Turbidity removal efficiency at GO dosage of 4 mg/L

Fig. 6 Optical microscopy images of **a** soil particles and **b** flocs with magnitude of 40 (initial turbidity: 162.5 NTU, pH: 6.5, GO dosage: 16.25 mg/L)
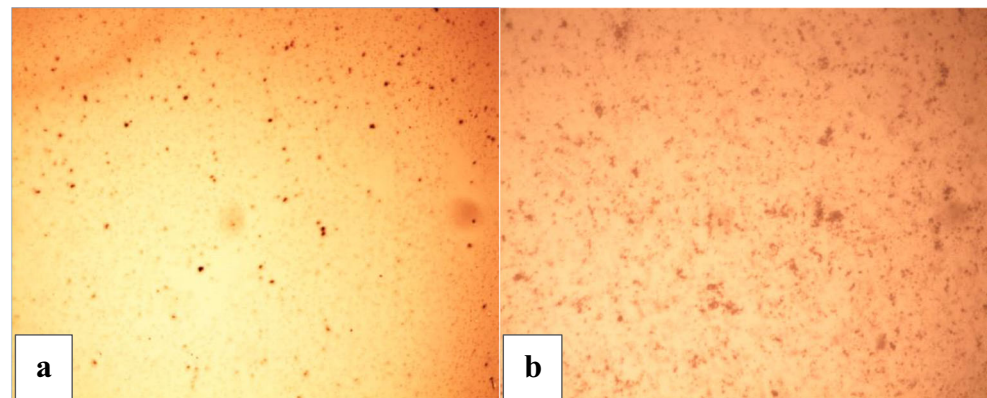
Fig. 7 SEM images of GO particles (**a**, **c**, **e**) and flocs (**b**, **d**, **f**), (initial turbidity: 162.5 NTU, pH: 6.5, GO dosage: 16.25 mg/L)

using 16.25 mg/L of GO. The figure illustrates the general shape of the soil particles and the formed flocs. The soil particles (Fig. 6a) seem discrete, small, and circular with vivid boundary; while it is observed that the flocs (Fig. 6b) are aggregated, larger, and irregular with no specific boundary.

To analyze the surface morphology and structural properties of GO and floc particles, SEM images were provided. The sheet-like and layered structure of the GO particles can be obviously seen in Fig. 7a, 7c, and 7e. In comparison, according to the SEM images of the floc particles (Fig. 7b, 7d, and
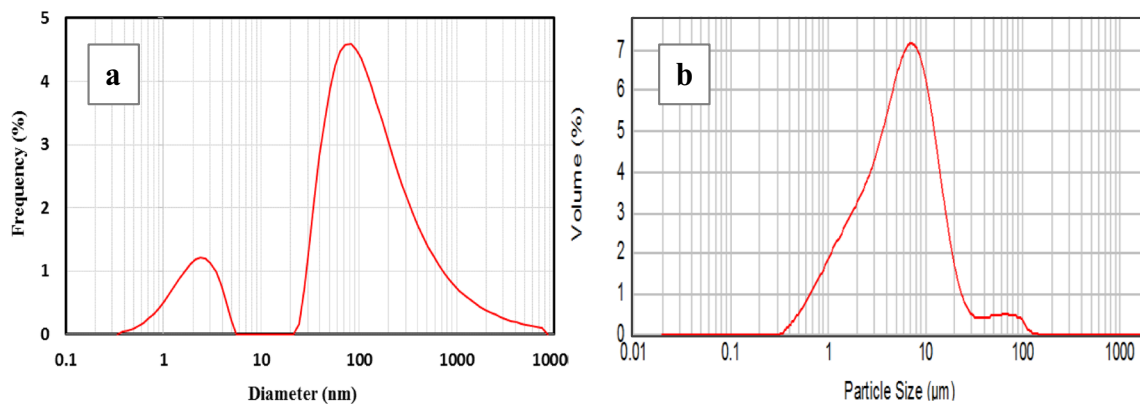
Fig. 8 Particle size distribution of **a** soil particles and **b** flocs (initial turbidity: 162.5 NTU, pH: 6.5, GO dosage: 16.25 mg/L)

7f), the layered structure is preserved, while the sheets cannot be observed more since they are filled with the soil particles. Furthermore, comparing the Fig. 7e and 7f indicates the agglomerated structure of the floc particles and their larger size than the GO particles. The microscopic images well illustrate the effectiveness of GO and its critical role as coagulant in turbidity removal from water.
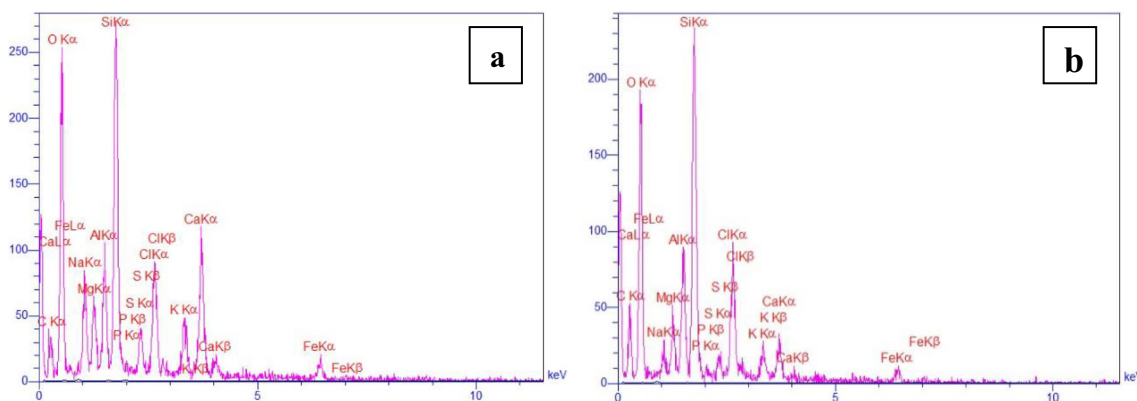
PSD analysis

In order to investigate the particle size distribution of the initial turbid sample as well as the formed flocs, the PSD analysis was performed on a sample before and after coagulation-flocculation process (initial turbidity, pH and GO dosage of 162.5 NTU, 6.5 and 16.25 mg/L, respectively). The results are depicted in Fig. 8. As seen in Fig. 8a, the PSD curve of the soil particles represents two classes of particles, one with a peak diameter of about 2.5 nm and a mean diameter of 2.1 nm, and the other with a peak at about 80 nm and a mean diameter of 298.8 nm. As the colloidal particle size range is between 1 and 1000 nm (Reynolds and Richards 1996), it can be said that a large proportion of the soil particles were colloidal. On the other hand, the PSD spectrum of the flocs (Fig. 8b) shows

one peak at 7 μm and has a mean diameter of 8.8 μm, which is much larger than those observed for the soil particles. The results indicate that the fine soil particles in both classes are coagulated in the form of large flocs.

EDX analysis

The EDX analysis was performed on the initial turbid sample and the settled flocs after coagulation-flocculation process. The results are presented in Fig. 9 and Table 7. The reason for the high oxygen content in the soil composition (58.15 W%) is the presence of mineral oxides. Silicon (Si), aluminum (Al), and magnesium (Mg) as the main constituents of clay and silt minerals were of the predominant mineral elements within the soil sample. Besides, the presence of phosphorus (P), sulfur (S), and carbon (C) elements was the sign of existence of organic matter and humus (Stevenson 1994; Sparks 2002). It can also be found from the data that all the elements detected in the soil sample were also present in the floc structure. This indicates that all the mineral oxides within the turbid sample have participated in the coagulation process and formation of the flocs using GO. However, it should be noted that the percentage of the elements was different in the two

Fig. 9 EDX analysis of **a** initial turbid sample and **b** flocs (initial turbidity: 162.5 NTU, pH: 6.5, GO dosage: 16.25 mg/L)

Table 7 The main constituents of soil and floc samples according to EDX analysis

Content as	Sample	Element												
		C	O	Na	Mg	Al	Si	P	S	Cl	K	Ca	Fe	Sum
W%[1]	Soil	20.51	58.15	4.88	2.36	2.60	6.05	0.11	0.69	1.73	0.83	1.80	0.29	100
	Floc	28.6	56.8	1.39	1.73	2.55	5.71	0.12	0.32	1.73	0.38	0.45	0.21	100
A%[2]	Soil	27.96	59.50	3.48	1.59	1.58	3.52	0.06	0.35	0.80	0.35	0.73	0.08	100
	Floc	36.95	55.05	0.94	1.10	1.46	3.15	0.06	0.15	0.75	0.15	0.17	0.06	100

[1] Weight percent, [2] Atomic percent

samples. For example, the carbon content of the floc particles was more than that of the soil particles. This is mainly attributed to the addition of GO particles to the floc structure. Due to the increased carbon contribution to the structure of the flocs, the percentage of most of the other elements such as Na, K, Ca, Mg, and Si decreased slightly.

Zeta potential analysis

Zeta potential (ZP) measurements were carried out on pH adjusted soil samples before coagulation and as well on floc samples formed during coagulation under two pH values of 6.5 and 3. As seen in Fig. 10a, the zeta potential of the soil environment at pH of 6.5 was about − 17.6 mV which slightly declined to − 16.3 mV in the floc environment. This negligible reduction of ZP indicates that the double layer compression could not be the main coagulation mechanism at pH of 6.5 while sweep coagulation and trapping of the particles played the main role in formation of the flocs.

Figure 10b shows the ZP values of the soil and the floc samples at the acidic pH of 3. In this case, the ZP of the soil environment was about − 15.3 mV, while it severely decreased to − 6 mV for the floc sample. Therefore, compared to ZP values obtained at pH 6.5, lower ZP values were obtained at pH 3 for both soil and floc environments. However, it is clear from the data that under pH 3, the presence of H^+ ions within the soil sample has resulted in a slight reduction of the ZP of the soil particles, while within the process environment (soil and GO particles), it severely decreased the formed flocs' ZP. This suggests that being surrounded both the soil and the GO particles by H^+ ions greatly reduced their charge intensity and the subsequent repulsion between them resulting in formation of flocs with lower ZP value. Undoubtedly, the very higher specific surface area of the GO nanoparticles, compared to that of the soil colloidal particles, has played a critical role in absorbance of large amounts of H^+ ions. Nevertheless, since both GO and soil particles still have the same charges and the ZP value of the flocs is not yet zero, it can be said that sweeping is still the main coagulation mechanism, while ZP reduction also contributed to the process.

Conclusions

Due to the unique properties of GO, researches on the application of this substance for removing contaminants
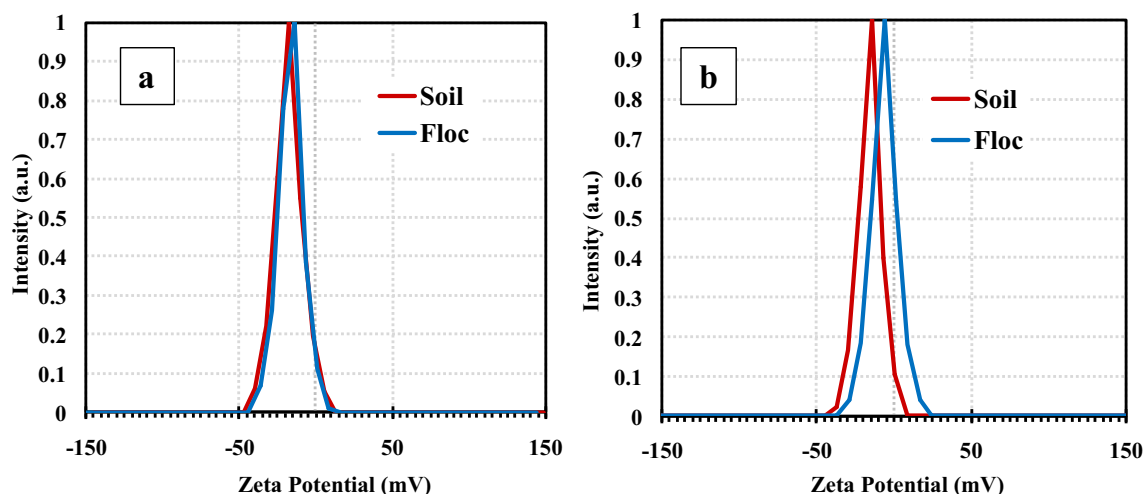
Fig. 10 ZP of soil and floc samples under **a** pH 6.5 and **b** pH 3 (initial turbidity: 162.5 NTU, GO dosage: 16.25 mg/L)

from the water environment have recently increased dramatically. Most of these researches have focused on GO performance as an adsorbent. However, very limited researches have been performed on GO performance as a coagulant. For this reason, its performance as a novel coagulating agent for turbidity removal from aqueous solution was aimed to be observed in a close scrutiny in the present work. According to the results, GO was highly effective as a coagulant in removing turbidity. Undoubtedly, large specific surface area of the GO sheets played a critical role in sweep coagulation of colloidal soil particles. Besides, under acidic pH conditions and abundance of H^+ ions, double layer compression and the subsequent ZP reduction also contributed to the process. A slight overdosing of GO and supernatant quality depletion was observed for dosages of more than 20 mg/L under pH values of less than about 4. The results of SEM, EDX, and PSD analyzes together with the optical microscope images proved the formation of the flocs on the layered structure of the GO particles. Although GO has not been used for water and wastewater treatment works yet, it is expected that after completing researches on its health effects, fully identifying its properties as a coagulant and producing the material in a cost-effective and large-scale manner, it will be considered as one of the strong alternatives to conventional coagulants for extensive use in treatment plants. As many of the coagulation properties of GO have not been investigated yet, the followings can be suggested to continue the research in this field:

– Examining the performance of GO with different structures, for example in terms of the number of layers, morphology, degree of oxidation, the amount of amorphization, etc.
– Combined use of GO and conventional coagulants and coagulant-aids
– Investigating the GO's coagulating effects on soluble pollutants such as heavy metals and humic substances in surface and ground waters
– Investigating the effect of sonication of GO suspension before coagulation-flocculation process
– Comparing the flocs, in terms of size, strength, and structure, formed through coagulation using GO and conventional coagulants

Compliance with ethical standards

References

Aboubaraka AE, Aboelfetoh EF, Ebeid EZM (2017) Coagulation effectiveness of graphene oxide for the removal of turbidity from raw surface water. Chemosphere 181:738–746. https://doi.org/10.1016/j.chemosphere.2017.04.137

Adesina OA, Abdulkareem F, Yusuff AS, Lala M, Okewale A (2019) Response surface methodology approach to optimization of process parameter for coagulation process of surface water using Moringa oleifera seed. S Afr J Chem Eng 28:46–51. https://doi.org/10.1016/j.sajce.2019.02.002

Altaher H (2012) The use of chitosan as a coagulant in the pre-treatment of turbid sea water. J Hazard Mater 233:97–102. https://doi.org/10.1016/j.jhazmat.2012.06.061

Anouzla A, Abrouki Y, Souabi S, Safi M, Rhbal H (2009) Colour and COD removal of disperse dye solution by a novel coagulant: application of statistical design for the optimization and regression analysis. J Hazard Mater 166:1302–1306. https://doi.org/10.1016/j.jhazmat.2008.12.039

Aslani H, Nabizadeh R, Nasseri S, Mesdaghinia A, Alimohammadi M, Mahvi AH, Rastkari N, Nazmara S (2016) Application of response surface methodology for modeling and optimization of trichloroacetic acid and turbidity removal using potassium ferrate (VI). Desalin Water Treat 57:25317–25328. https://doi.org/10.1080/19443994.2016.1147380

Baghvand A, Zand AD, Mehrdadi N, Karbassi A (2010) Optimizing coagulation process for low to high turbidity waters using aluminum and iron salts. Am J Environ Sci 6:442–448. https://doi.org/10.3844/ajessp.2010.442.448

Bolt GH (1976) Adsorption of anions by soil. Dev Soil Sci 5:91–95. https://doi.org/10.1016/S0166-2481(08)70634-2

Daud NM, Sheikh Abdullah SR, Abu Hasan H (2018) Response surface methodological analysis for the optimization of acid-catalyzed transesterification biodiesel wastewater pre-treatment using coagulation–flocculation process. Process Saf Environ 113:184–192. https://doi.org/10.1016/j.psep.2017.10.006

Divakaran R, Pillai VS (2002) Flocculation of river silt using chitosan. Water Res 36:2414–2418. https://doi.org/10.1016/S0043-1354(01)00436-5

Guo B, Yu H, Gao B, Rong H, Dong H, Ma D, Li R, Zhao S (2015) Coagulation performance and floc characteristics of aluminum sulfate with cationic polyamidine as coagulant aid for kaolin-humic acid treatment. Colloids and Surfaces A: Physicochemical and Engineering Aspects 48:476–484. https://doi.org/10.1016/j.colsurfa.2015.06.017

Hiew BYZ, Lee LY, Lai KC, Gan S, Thangalazhy-Gopakumar S, Pan GT, Yang TCK (2019) Adsorptive decontamination of diclofenac by three-dimensional graphene-based adsorbent: response surface methodology, adsorption equilibrium, kinetic and thermodynamic studies. Environ Res 168:241–253. https://doi.org/10.1016/j.envres.2018.09.030

Huang X, Zhao Y, Gao B, Sun S, Wang Y, Li Q, Yue Q (2016) Polyacrylamide as coagulant aid with polytitanium sulfate in humic acid-kaolin water treatment: effect of dosage and dose method. J Taiwan Inst Chem Eng 64:173–179. https://doi.org/10.1016/j.jtice.2016.04.011

Hummers WS Jr, Offeman RE (1958) Preparation of graphitic oxide. J Am Chem Soc 80:1339. https://doi.org/10.1021/ja01539a017

Jefferson B, Sharp EL, Goslan E, Henderson R, Parsons SA (2004) Application of charge measurement to water treatment processes. Water Sci Technol: Water Supply 4:49–56. https://doi.org/10.2166/ws.2004.0092

Jiang JQ (2015) The role of coagulation in water treatment. Curr Opin Chem Eng 8:36–44. https://doi.org/10.1016/j.coche.2015.01.008

Jiang JQ, Wang HY (2009) Comparative coagulant demand of polyferric chloride and ferric chloride for the removal of humic acid. Sep Sci Technol 44:386–397. https://doi.org/10.1080/01496390802590020

Jin L, Chai L, Ren L, Jiang Y, Yang W, Wang S, Liao Q, Wang H, Zhang L (2019) Enhanced adsorption-coupled reduction of hexavalent chromium by 2D poly (m-phenylenediamine)-functionalized reduction graphene oxide. Environ Sci Pollut Res 26:31099–31110. https://doi.org/10.1007/s11356-019-06175-x

Kang M, Kameib T, Magarab Y (2003) Comparing polyaluminum chloride and ferric chloride for antimony removal. Water Res 37:4171–4179. https://doi.org/10.1016/S0043-1354(03)00351-8

Kirmizakis P, Tsamoutsoglou C, Kayan B, Kalderis D (2014) Subcritical water treatment of landfill leachate: application of response surface methodology. J Environ Manage 146:9–15. https://doi.org/10.1016/j.jenvman.2014.04.037

Krishnan S, Zulkapli NS, Din MFM, Majid ZA, Honda M, Ichikawa Y, Sairan FM, Nasrullah M, Guntor NAA (2020) Statistical optimization of titanium recovery from drinking water treatment residue using response surface methodology. J Environ Manage 255:109890. https://doi.org/10.1016/j.jenvman.2019.109890

Li Z, Chen F, Yuan L, Liu Y, Zhao Y, Chai Z, Shi W (2012) Uranium (VI) adsorption on graphene oxide nanosheets from aqueous solutions. Chem Eng J 210:539–546. https://doi.org/10.1016/j.cej.2012.09.030

Liu G, Han K, Ye H, Zhu C, Gao Y, Liu Y, Zhou Y (2017) Graphene oxide/triethanolamine modified titanate nanowires as photocatalytic membrane for water treatment. Chem Eng J 320:74–80. https://doi.org/10.1016/j.cej.2017.03.024

Metcalf & Eddy (2003) Wastewater engineering: treatment and reuse, 4th edn. McGraw-Hill, New York

Montgomery DC (2001) Design and analysis of experiments, 5th edn. John Wiley & Sons, New York

Mora BP, Bellú S, Mangiameli MF, Frascaroli MI, González JC (2019) Response surface methodology and optimization of arsenic continuous sorption process from contaminated water using chitosan. J Water Process Eng 32:100913. https://doi.org/10.1016/j.jwpe.2019.100913

Myers RH, Montgomery DC, Anderson-Cook CM (2009) Response surface methodology: process and product optimization using designed experiments, 3rd edn. John Wiley & Sons, New York

Nourani M, Baghdadi M, Javan M, Bidhendi GN (2016) Production of a biodegradable flocculant from cotton and evaluation of its performance in coagulation-flocculation of kaolin clay suspension: Optimization through response surface methodology (RSM). J Environ Chem Eng 4:1996–2003. https://doi.org/10.1016/j.jece.2016.03.028

Ooi TY, Yong EL, Din MF, Rezania S, Aminudin E, Chelliapan S, Rahman AA, Park J (2018) Optimization of aluminium recovery from water treatment sludge using response surface methodology. J Environ Manage 228:13–19. https://doi.org/10.1016/j.jenvman.2018.09.008

Park S, Ruoff RS (2009) Chemical methods for the production of graphenes. Nat Nanotechnol 4:217–224. https://doi.org/10.1038/nnano.2009.58

Qasim SR, Motley EM, Zhu G (2002) Water works engineering: planning design and operation, 1st ed., prentice Hall

Ramesha G, Kumara AV, Muralidhara H, Sampath S (2011) Graphene and graphene oxide as effective adsorbents toward anionic and cationic dyes. J Colloid Interface Sci 361:270–277. https://doi.org/10.1016/j.jcis.2011.05.050

Reynolds TD, Richards PA (1996) Unit operations and processes in environmental engineering, 2nd edn. PWS Publishing Company, Boston

Rizzo L, Belgiomo V, Gallo M, Meric S (2005) Removal of THM precursors from a high-alkaline surface water by enhanced coagulation and behaviour of THMFP toxicity on D. magna. Desalination 176:177–188. https://doi.org/10.1016/j.desal.2004.10.020

Rizzo L, Di Gennaro A, Gallo M, Belgiorno V (2008) Coagulation/chlorination of surface water: a comparison between chitosan and metal salts. Sep Purif Technol 62:79–85. https://doi.org/10.1016/j.seppur.2007.12.020

Robati D, Mirza B, Rajabi M, Moradi O, Tyagi I, Agarwal S, Gupta V (2016) Removal of hazardous dyes-BR 12 and methyl orange using graphene oxide as an adsorbent from aqueous phase. Chem Eng J 284:687–697. https://doi.org/10.1016/j.cej.2015.08.131

Sadri Moghaddam S, Alavi Moghaddam M, Arami M (2011) Response surface optimization of acid red 119 dye from simulated wastewater using Al based waterworks sludge and polyaluminium chloride as coagulant. J Environ Manage 92:1284–1291. https://doi.org/10.1016/j.jenvman.2010.12.015

Sanchez VC, Jachak A, Hurt RH, Kane AB (2011) Biological interactions of graphene-family nanomaterials: an interdisciplinary review. Chem Res Toxicol 25:15–34. https://doi.org/10.1021/tx200339h

Simate GS, Iyuke SE, Ndlovu S, Heydenrych M (2012) The heterogeneous coagulation and flocculation of brewery wastewater using carbon nanotubes. Water Res 46:1185–1197. https://doi.org/10.1016/j.watres.2011.12.023

Sparks DL (2002) Environmental Soil Chemistry, 2nd ed., Academic Press

Stevenson FJ (1994) Humus chemistry: genesis, composition, reactions, 2nd ed., John Wiley & Sons, New York

Tan P, Bi Q, Hu Y, Fang Z, Chen Y, Cheng J (2017) Effect of the degree of oxidation and defects of graphene oxide on adsorption of Cu^{2+} from aqueous solution. Appl Surf Sci 423:1141–1151. https://doi.org/10.1016/j.apsusc.2017.06.304

Trinh TK, Kang LS (2011) Response surface methodological approach to optimize the coagulation–flocculation process in drinking water treatment. Chem Eng Res Des 89:1126–1135. https://doi.org/10.1016/j.cherd.2010.12.004

Van Benschoten JE, Edzwald JK (1990) Chemical aspects of coagulation using aluminum salts i. hydrolytic reactions of alum and polyaluminum chloride. Water Res 24(12):1519–1526. https://doi.org/10.1016/0043-1354(90)90086-L

Yang ZL, Gao BY, Yue QY, Wang Y (2010) Effect of pH on the coagulation performance of Al-based coagulants and residual aluminum speciation during the treatment of humic acid–kaolin synthetic water. J Hazard Mater 178:596–603. https://doi.org/10.1016/j.jhazmat.2010.01.127

Yang ST, Chen S, Chang Y, Cao A, Liu Y, Wang H (2011) Removal of methylene blue from aqueous solution by graphene oxide. J Colloid Interface Sci 359:24–29. https://doi.org/10.1016/j.jcis.2011.02.064

Yang X, Chen C, Li J, Zhao G, Ren X, Wang X (2012a) Graphene oxide-iron oxide and reduced graphene oxide-iron oxide hybrid materials for the removal of organic and inorganic pollutants. RSC Adv 2: 8821–8826. https://doi.org/10.1039/C2RA20885G

Yang Z, Yuan B, Huang X, Zhou J, Cai J, Yang H, Li A, Cheng R (2012b) Evaluation of the flocculation performance of carboxymethyl chitosan-graft-polyacrylamide, a novel amphoteric chemically bonded composite flocculant. Water Res 46:107–114. https://doi.org/10.1016/j.watres.2011.10.024

Yang Z, Yan H, Yang H, Li H, Li A, Cheng R (2013) Flocculation performance and mechanism of graphene oxide for removal of various contaminants from water. Water Res 47:3037–3046. https://doi.org/10.1016/j.watres.2013.03.027

Zhang HF, Sun BS, Zhao XH, Gao ZH (2008) Effect of ferric chloride on fouling in membrane bioreactor. Sep Purif Technol 63:341–347. https://doi.org/10.1016/j.seppur.2008.05.024

Zhao G, Jiang L, He Y, Li J, Dong H, Wang X, Hu W (2011a) Sulfonated graphene for persistent aromatic pollutant management. Adv Mater 23:3959–3963. https://doi.org/10.1002/adma.201101007

Zhao G, Li J, Ren X, Chen C, Wang X (2011b) Few-layered graphene oxide nanosheets as superior sorbents for heavy metal ion pollution management. Environ Sci Technol 45:10454–10462. https://doi.org/10.1021/es203439v

Zhao Z, Sun W, Ray MB, Ray AK, Huang T, Chen J (2019) Optimization and modeling of coagulation-flocculation to remove algae and organic matter from surface water by response surface methodology. Front Environ Sci Eng 13(5):75. https://doi.org/10.1007/s11783-019-1159-7

Zhu G, Zheng H, Zhang Z, Tshukudu T, Zhang P, Xiang X (2011) Characterization and coagulation–flocculation behavior of polymeric aluminum ferric sulfate (PAFS). Chem Eng J 178:50–59. https://doi.org/10.1016/j.cej.2011.10.008